Fusion reaction studies for the ^{6}Li + ^{124}Sn system at near-barrier energies

V. V. Parkar,[1,*] S. K. Pandit,[1,2] A. Shrivastava,[1,2] R. Palit,[3] K. Mahata,[1,2] V. Jha,[1,2] K. Ramachandran,[1] Shilpi Gupta,[1,2] S. Santra,[1,2] Sushil K. Sharma,[3,†] S. Upadhyaya,[4,†] T. N. Nag,[5] Sutanu Bhattacharya,[6] T. Trivedi,[6] and S. Kailas[1,7]

[1]*Nuclear Physics Division, Bhabha Atomic Research Centre, Mumbai 400085, India*
[2]*Homi Bhabha National Institute, Anushaktinagar, Mumbai 400094, India*
[3]*Department of Nuclear and Atomic Physics, Tata Institute of Fundamental Research, Mumbai 400005, India*
[4]*Department of Applied Physics, Amity University, Noida 201313, India*
[5]*Radiochemistry Division, Bhabha Atomic Research Centre, Mumbai 400085, India*
[6]*Department of Pure and Applied Physics, Guru Ghasidas Vishwavidyalaya, Bilaspur 495009, India*
[7]*UM-DAE Centre for Excellence in Basic Sciences, Mumbai 400098, India*

(Received 9 April 2018; published 3 July 2018)

The complete and incomplete fusion along with one neutron stripping and pickup cross sections for the ^{6}Li + ^{124}Sn system are measured using online and offline characteristic γ-ray detection techniques. The complete fusion (CF) cross sections at energies above the Coulomb barrier are found to be suppressed by ∼34% compared to the coupled channel calculations. This suppression observed in complete fusion cross sections is found to be commensurate with the measured total incomplete fusion (ICF) cross sections. There is a distinct feature observed in the ICF cross sections, i.e., d capture is found to be dominant than α capture at all the measured energies, contrary to the data available for ^{6}Li + ^{209}Bi,^{197}Au systems. The total fusion cross section ratio between ^{6}Li and ^{7}Li induced reactions shows an increasing trend as the energy decreases below the barrier while it remains unity at above-barrier energies. A simultaneous explanation of complete, incomplete, and total fusion (TF) data is also obtained from the calculations based on the continuum discretized coupled channel method with short-range imaginary potentials. The cross section ratios of CF/TF and ICF/TF obtained from the data as well as the calculations shows the dominance of ICF at below-barrier energies and CF at above-barrier energies.

DOI: 10.1103/PhysRevC.98.014601

I. INTRODUCTION

Exploring the influence of the weakly bound cluster structure of light nuclei in reaction dynamics is a topic of current interest [1,2]. The low breakup threshold of such nuclei leads to breakup into the constituent cluster fragments, resulting in suppression of complete fusion [3–5], breakup threshold anomaly in the optical potential [6–8], large inclusive breakup α cross sections [9–11], etc. Large α yields relative to the complementary fragments for nuclear reactions involving nuclei with $\alpha + x$ cluster structure, e.g., ^{6,8}He, ^{6,7}Li, ^{7,9}Be, are observed. In recent studies, it was found that the t capture process is the main source of α production in the reactions involving ^{7}Li nuclei [10]. For ^{6}Li induced reactions, it is also claimed that d capture is the main source of α yields [11]. In reactions involving ^{7}Li nuclei, the measured t capture cross sections are larger than α capture cross sections over a wide energy range [12–14]. However, in the reactions involving ^{6}Li nuclei, the limited available data with ^{209}Bi [15] and ^{197}Au [16] targets showed that the d capture cross sections are larger than α capture cross sections at below-barrier energies, while α capture and d capture cross sections are of similar order at above-barrier energies. Hence, a complete set of measurements and comparison of α and d/t capture cross sections with ^{6,7}Li projectiles on the same target are essential to understand these differences.

Except for the ^{209}Bi and ^{197}Au targets, the complete set of fusion data with both ^{6,7}Li projectiles has not been measured. For the ^{7}Li + ^{159}Tb system, the CF, t capture, and α capture cross sections were measured [17]. Similarly, for the ^{6}Li + ^{159}Tb system, the CF, d capture and partial α capture cross sections were measured [18]. Hence, the remaining residues from α capture need to be measured for unambiguous comparison of α and d capture cross sections. Recently, we reported the complete set of fusion data for the ^{7}Li + ^{124}Sn system [14].

In the present work, the effects of the cluster structure on the reaction dynamics are reported from comparative study of complete (CF) and incomplete fusion (ICF) processes involving ^{6,7}Li projectiles. We report the measurement of CF and ICF along with one-neutron stripping and pickup cross sections for the ^{6}Li + ^{124}Sn system around the Coulomb barrier energies, utilizing both online and offline characteristic γ-ray detection techniques. The dominant evaporation residues (ERs) from complete fusion are ^{127}I ($3n$) and ^{126}I ($4n$). In addition, we also identified the residues from α capture, populating ^{126,127}Te in online measurement. In the present case, the residue ^{126}I ($4n$) along with the residues following d capture, viz., ^{124}Sn(d,$1n$)^{125}Sb, ^{124}Sn(d,$2n$)^{124}Sb, and transfer

*vparkar@barc.gov.in
†Present address: The Marian Smoluchowski Institute of Physics, Jagiellonian University, Łojasiewicza 11, 30-348 Kraków, Poland.

products ^{125}Sn (one-neutron stripping) and ^{123}Sn (one-neutron pickup) undergo radioactive decay with half-lives suitable for offline measurements. The offline γ-ray activity measurements were carried out after irradiation of the target with different beam energies for extraction of cross sections of these residues to get complete information of total ICF and $1n$ transfer channels. For ^{126}I, it was possible to obtain the cross sections using both in-beam and off-beam methods. In addition to this, we also measured the residue cross sections from α capture (in the off-beam method) at a few energies which were not measured in earlier work [18] in the ^{6}Li + ^{159}Tb system.

The paper is organized as follows: the experimental details are described in Sec. II. The experimental results, systematics of data, along with coupled channel calculations are given in Sec. III. The summary of the present study is given in Sec. IV.

II. EXPERIMENTAL DETAILS

Two separate experiments were carried out for in-beam and off-beam γ-ray counting using the ^{6}Li beam at the 14UD BARC-TIFR Pelletron-Linac accelerator facility, Mumbai. A detailed description of the experimental setup used for online γ-ray measurements is given in our earlier works [3,14] and only a short summary pertinent to this work is presented here. The ^{6}Li beam with energies $E_{\rm beam}$ = 18–36 MeV in 1–2 MeV steps was bombarded on a ^{124}Sn target (thickness = 2.47 ± 0.04 mg/cm^2). The beam energies were corrected for the loss at half the target thickness and used in the further analysis. A Compton suppressed clover detector placed at 125° at a distance of 25 cm from the target center was used for the estimation of absolute cross section of populated reaction channels. The absolute efficiency of this detector was determined using a set of radioactive ^{152}Eu, ^{133}Ba, and ^{241}Am sources mounted in the same geometry as the target. Along with the clover detector, one Si surface barrier detector (thickness 500 μm) was placed at 30° to monitor Rutherford scattering for absolute normalization purposes. The integrated beam current deposited at the beam dump after the target was also recorded using a high precision current integrator.

For the off-beam measurement, three targets of ^{124}Sn having thicknesses 3.3, 1.7 and 3.2 mg/cm^2 were irradiated with beam of ^{6}Li at 20.2, 25.9, and 34.2 MeV energies respectively. These energies were chosen in such a way that, after energy loss correction at half the target thickness, they match with that of previously measured online γ-ray measurements. The targets, with the Al catcher (∼1 mg/cm^2 thick), were placed normal to the beam direction so that the recoiling residues were stopped in the target-catcher assembly and were irradiated for almost 18 h. The beam current was ∼80 nA and it was monitored and recorded using a computer-aided measurement and control (CAMAC) scaler every minute during each irradiation. The irradiated target-catcher assembly was attached to a perspex sheet and kept at a fixed distance (∼10 cm) in front of a high-purity germanium (HPGe) detector for counting. The HPGe detector was surrounded by 2 mm thick Cu and Cd sheets and 5 cm thick Pb sheets to reduce the background. The energy calibration and absolute efficiency of the HPGe detector were measured using a set of calibrated radioactive ^{152}Eu, ^{133}Ba, and ^{241}Am sources placed at the same geometry as the target.

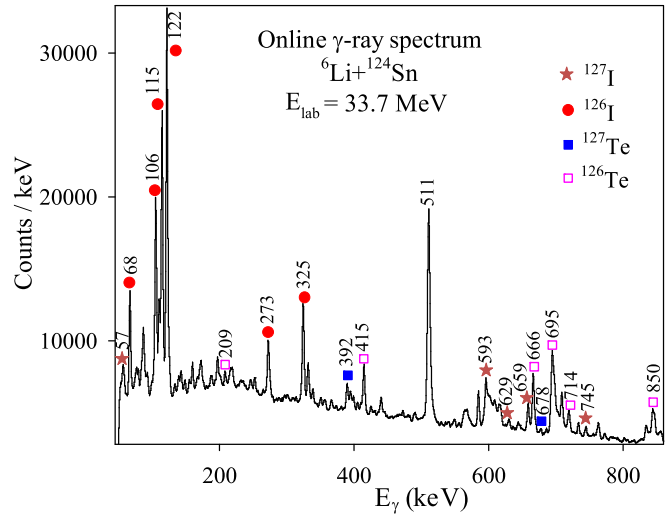

FIG. 1. γ-ray add-back spectrum from the Compton suppressed clover detector at 125° obtained in the ^{6}Li + ^{124}Sn system at $E_{\rm lab}$ = 33.7 MeV. The γ lines from the possible evaporation residues (^{126,127}I) following CF are labeled. Also the γ lines following the α capture channel (^{126,127}Te) are marked.

All three targets were counted individually at various intervals following the half lives. In addition, four targets of ^{159}Tb having thicknesses 1.7–1.9 mg/cm^2 were irradiated with the ^{6}Li beam at 24, 26.1, 25.9, and 30.1 MeV energies for measurement of residue cross sections from α capture.

III. RESULTS AND DISCUSSION

A typical in-beam γ-ray add-back spectrum at $E_{\rm lab}$ = 33.7 MeV is shown in Fig. 1. The γ lines from the ERs following CF, viz., ^{126,127}I, are labeled. Also the identified γ lines following the ICF channel, viz., from α capture, ^{126,127}Te, are marked. The typical off-beam γ-ray spectrum at $E_{\rm lab}$ = 33.7 MeV is shown in Fig. 2, where the residues from CF, d capture, and $1n$ transfer identified by the characteristic γ lines are labeled. The decay half-lives ($T_{1/2}$) and intensities are same as listed in our previous work on the ^{7}Li + ^{124}Sn system [14].

A. Complete fusion

The cross sections for the residues from complete fusion, ^{127}I ($3n$) and ^{126}I ($4n$), obtained using the prompt γ-ray transitions are shown in Fig. 3. The cross sections of γ-ray transitions feeding to the ground and metastable (having lifetimes of a few μs) states of the particular residue are added to get the residue cross sections. The information of γ lines populating the ground and metastable states in these nuclei is taken from Refs. [19,20]. ^{126}I is also a β-active nucleus ($T_{1/2}$ = 12.93 days) and hence the cross sections for this channel were obtained by following the radioactive decay in the off-beam γ-ray counting method and are found to be consistent with the in-beam measurements as shown by the open circle symbol in Fig. 3. The statistical model predictions using the PACE code [21] are also shown in Fig. 3. The angular

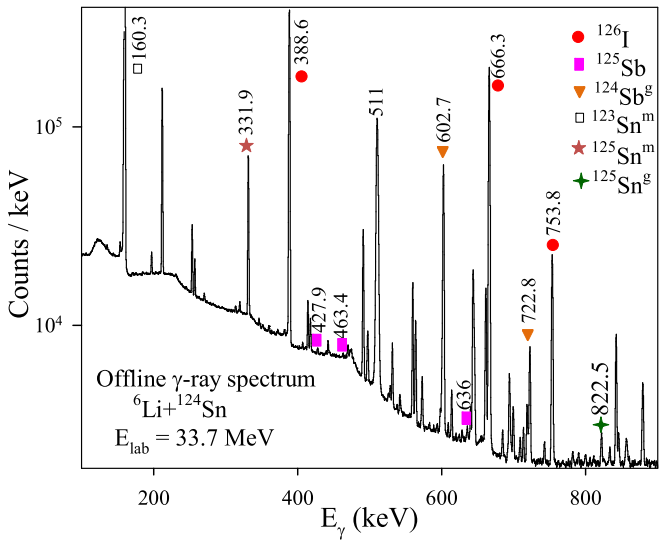

FIG. 2. Offline γ-ray spectrum obtained in the HPGe detector for the ^{6}Li + ^{124}Sn system at $E_{lab} = 33.7$ MeV. Identified γ lines from different residues following CF (^{126}I), d capture (^{124,125}Sb), one-neutron stripping (^{125}Sn), and one-neutron pickup (^{123}Sn) are marked.

momentum distribution obtained from the coupled channel code CCFULL [22] was used as input in PACE at each energy to obtain the cross sections of the decay channels.

The complete fusion cross sections were determined by dividing the cumulative measured (σ^{expt}_{3n+4n}) cross sections by the ratio R, which gives the missing ER contribution, if any. Here the ratio R is defined as $R = \sum_{x} \sigma^{PACE}_{xn} / \sigma^{PACE}_{fus}$, where

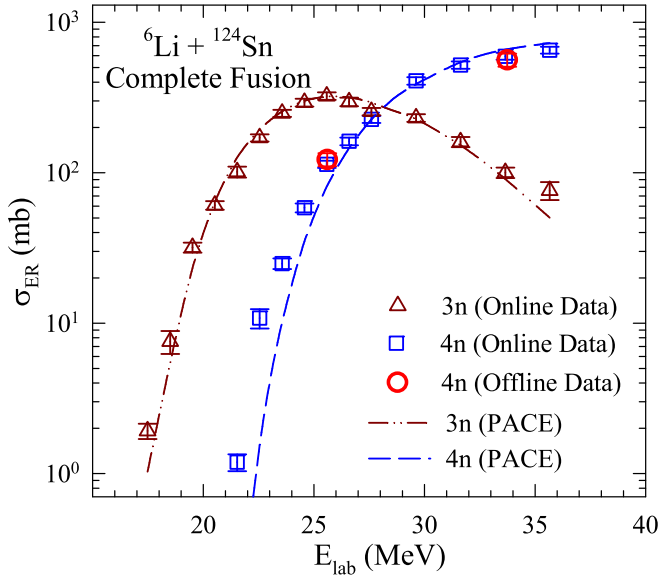

FIG. 3. ER cross sections from online γ-ray measurement for $3n$ (^{127}I) and $4n$ (^{126}I) channels following CF are represented by open triangles and open squares, respectively. The ER data from offline γ-ray measurement for the $4n$ channel are also shown by open circles. The results of the statistical model calculations for the corresponding ERs are shown by dash-dot-dot ($3n$) and dashed ($4n$) lines.

TABLE I. Measured cross sections for $\Sigma\sigma_{xn}$ ($x = 3,4$) evaporation residues and complete fusion along with the ratio R, obtained from PACE (defined in the text) for the ^{6}Li + ^{124}Sn system for the measured energy range.

E_{lab} (MeV)	$E_{c.m.}$ (MeV)	σ^{expt}_{3n+4n} (mb)	R (PACE)	σ^{expt}_{CF} (mb)
17.5	16.7	1.92 ± 0.22	0.79	2.43 ± 0.28
18.5	17.6	7.55 ± 1.31	0.87	8.68 ± 1.50
19.5	18.6	31.9 ± 2.44	0.92	34.7 ± 2.7
20.5	19.6	60.8 ± 4.0	0.95	64.1 ± 4.2
21.5	20.5	103 ±9	0.97	106 ± 9
22.6	21.5	182 ±10	0.98	186 ± 10
23.6	22.5	273 ± 14	0.98	278 ± 14
24.6	23.4	351 ±18	0.99	356 ± 18
25.6	24.4	438 ±19	0.99	443 ± 20
26.6	25.4	458 ±22	0.99	464 ± 22
27.6	26.3	482 ±19	0.99	488 ± 19
29.6	28.3	639 ± 27	0.99	648 ± 27
31.6	30.2	680 ±31	0.98	692± 32
33.7	32.1	695 ±32	0.98	712 ± 33
35.7	34.0	729 ±36	0.94	773 ± 39

$x = 3,4$. The CF cross sections thus obtained are listed in Table I and plotted in Fig. 4. The error bars on the data are due to statistics, background subtraction, and absolute efficiency of the detectors. For off-beam measurements, uncertainty in the target thickness was also included.

Coupled channel (CC) calculations were performed using the code CCFULL [22]. The potential parameters used were $V_0 = 45$ MeV, $r_0 = 1.17$ fm, and $a_0 = 0.61$ fm, obtained from the Woods-Saxon parametrization of the Akyuz-Winther

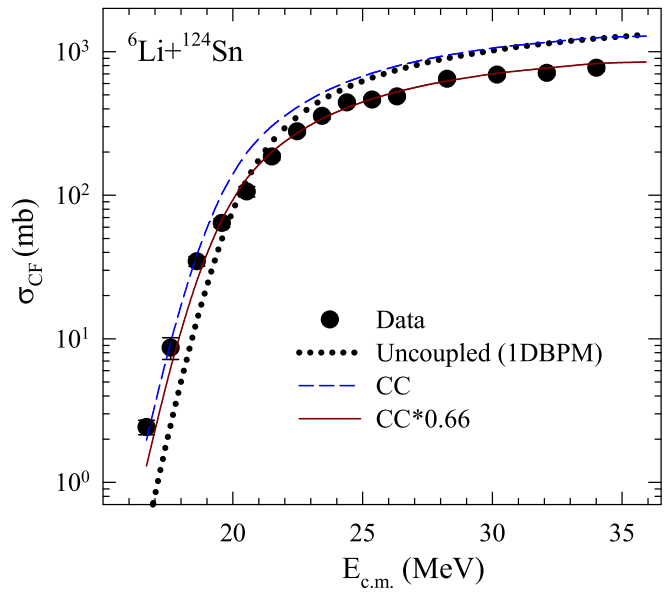

FIG. 4. Complete fusion cross section (filled circles) for the ^{6}Li + ^{124}Sn system compared with coupled (dashed lines) and uncoupled (dotted lines) results from CCFULL calculations. Solid lines were obtained by multiplying the coupled results by a factor of 0.66.

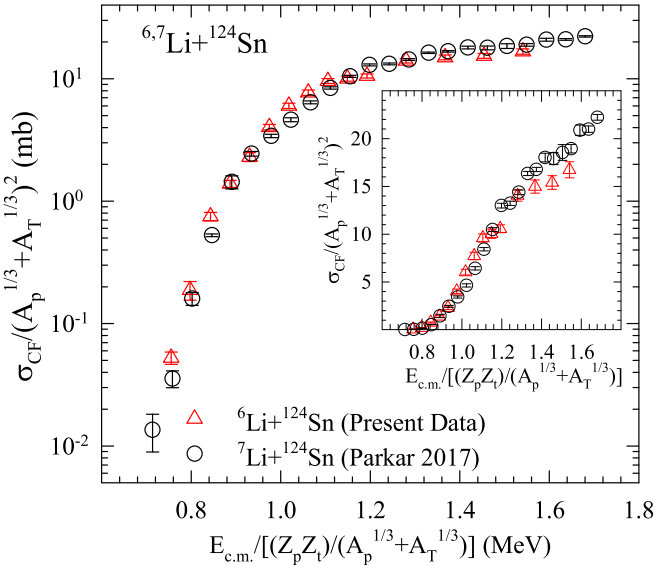

FIG. 5. Comparison of measured CF cross sections in reduced scale vs reduced energy for ^{6,7}Li + ^{124}Sn systems plotted in logarithmic and linear (in the inset) scales (see text for details).

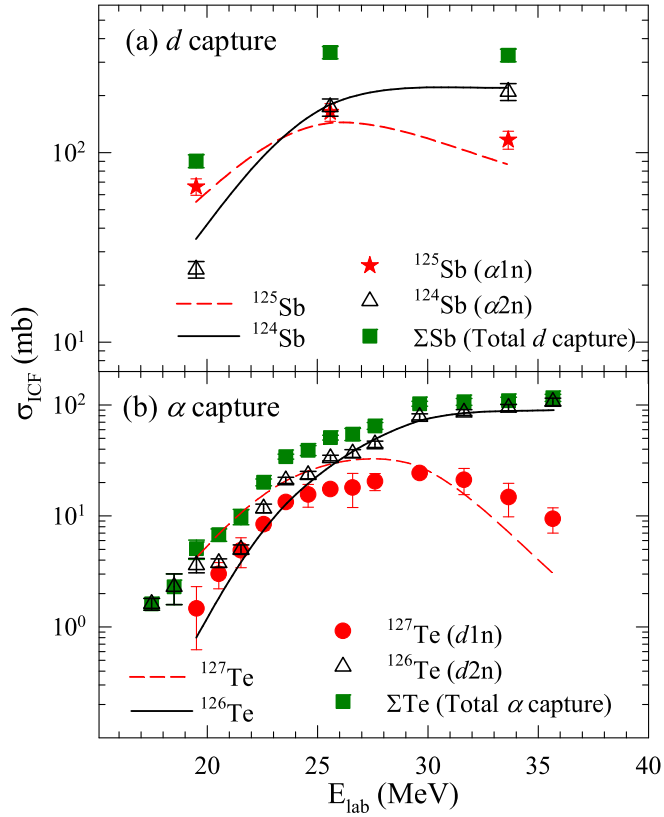

FIG. 6. Measured residue cross sections for (a) d capture (from offline γ-ray measurement) (b) α capture (from online γ-ray measurement) in the ^{6}Li + ^{124}Sn system are plotted. The lines are the predictions from statistical model calculations for the corresponding residues (see text for details).

(AW) potential [23]. The corresponding uncoupled barrier height V_B, radius R_B, and curvature $\hbar\omega$ derived for the present systems are 20.0 MeV, 10.1 fm, and 4.53 MeV respectively. The CC calculations include two target inelastic vibrational states, 2^+, 1.132 MeV and 3^-, 2.603 MeV with $\beta_2 = 0.0953$ and $\beta_3 = 0.106$ [24] respectively. The projectile ground state (1^+) having the quadrupole moment $Q = -0.082$ fm^2 [25] was also coupled along with these two target inelastic states.

The results of the CC calculations are shown in Fig. 4. It can be seen from Fig. 4 that, at energies below the barrier, the CC calculations (dashed line) show an enhancement of fusion cross section as compared to the uncoupled ones (dotted lines). However, at above-barrier energies, the calculated values of fusion with or without couplings are higher than the measured ones. The measured fusion cross sections agree very well with the calculated ones when multiplied by a factor of 0.66 (solid line). This implies that there is an overall suppression of the complete fusion cross section by ∼34% as compared to the ones predicted by CCFULL. An uncertainty of 4% in suppression factor was estimated from the uncertainties in V_B and σ_{CF}. This value of suppression in CF is found to be independent of target, in agreement with the data available from the literature [4,5] with weakly bound projectiles.

In Fig. 5, we show the comparison of measured CF cross sections in reduced scale, $\sigma_{CF}/(A_p^{\frac{1}{3}} + A_t^{\frac{1}{3}})^2$, vs reduced energy $E_{\rm c.m.}/[(Z_pZ_t)/(A_p^{\frac{1}{3}} + A_t^{\frac{1}{3}})]$ for the two projectiles ^{6,7}Li on a ^{124}Sn target in the logarithmic and linear (in the inset) scales. The corresponding cross sections involving the ^{7}Li projectile are taken from Ref. [14]. It was observed that the CF cross sections with ^{7}Li at above-barrier energies are larger than those with ^{6}Li, which is consistent with the values of break up thresholds. However, at below-barrier energies, the cross sections with ^{6}Li are higher than those with ^{7}Li. A similar observation is also made in the work of Rath *et al.* with ^{6,7}Li + ^{144,152}Sm systems [26].

B. ICF and 1n transfer cross sections

We have also identified the residues from incomplete fusion and one-neutron transfer channels and extracted the cross sections. The cross sections for the residues from α capture, ^{126,127}Te, were obtained from prompt γ-ray transitions. The γ lines for these nuclei were identified from Ref. [27]. The cross sections for the residues from d capture (^{124,125}Sb) and 1n transfer (^{123,125}Sn) were obtained by following the radioactive decay in the off-beam γ-ray measurement. In Table II, the measured cross sections for incomplete fusion (^{126,127}Te and ^{124,125}Sb residues) along with one-neutron pickup (^{123}Sn) and stripping (^{125}Sn) products are given. These measured cross sections for residues from d capture and α capture are shown in Figs. 6(a) and 6(b), respectively. Similarly for ^{6}Li + ^{159}Tb system, the cross sections for the residues from α capture are listed in Table III. Note that proton pickup in the target would give the same ER as the one following d capture process and subsequent few neutron evaporation. Hence, from experiments it is difficult to separate these two processes.

In order to investigate the behavior in observed residues from d capture and α capture in the ^{6}Li + ^{124}Sn system,

TABLE II. Measured cross sections for residues from incomplete fusion, 1n pickup and 1n stripping reactions obtained from online and offline γ-ray measurements in ^{6}Li + ^{124}Sn system.

E_{lab} (MeV)	^{127}Te (mb)	^{126}Te (mb)	^{125}Sb (mb)	^{124}Sb^{g} (mb)	^{125}Sn^{g} (mb)	^{125}Sn^{m} (mb)	^{123}Sn^{m} (mb)
17.5		1.61 ± 0.20					
18.5		2.30 ± 0.71					
19.5	1.47 ± 0.84	3.61 ± 0.54	66.2 ± 6.6	24.2 ± 2.4	4.40 ± 0.51	10.2 ± 1.1	6.22 ± 0.63
20.5	3.00 ± 0.80	3.77 ± 0.33					
21.5	4.90 ± 1.47	5.00 ± 0.50					
22.6	8.41 ± 0.98	11.7 ± 1.1					
23.6	13.3 ± 1.1	21.0 ± 1.3					
24.6	15.6 ± 3.6	23.4 ± 1.8					
25.6	17.5 ± 1.6	33.3 ± 2.0	164 ± 18	174 ± 18	20.1 ± 2.1	27.8 ± 2.8	36.7 ± 3.7
26.6	18.1 ± 6.1	36.6 ± 2.9					
27.6	20.5 ± 3.6	44.3 ± 2.9					
29.6	24.4 ± 2.1	78.3 ± 4.9					
31.6	21.2 ± 5.7	85.7 ± 5.0					
33.7	14.8 ± 4.9	94.7 ± 6.1	117 ± 13	210 ± 22	22.8 ± 2.4	23.8 ± 2.4	37.4 ± 4.6
35.7	9.4 ± 2.4	107 ± 8					

statistical model calculations using PACE [21] code were performed. The code is modified accordingly for particle evaporations from the composite systems formed in fragment-capture reactions. The details are available in Ref. [28]. In the case of compound nucleus formation, the excitation energy of the compound nucleus is $E^{*} = Q_{gg} + E_{c.m.}$, which is a fixed value for a particular incident beam energy. However, the excitation energy of the composite system in fragment capture reactions has a wider distribution. The shape of the distribution can be estimated by measuring the energy spectra of the outgoing complementary cluster fragment. Typically 10 MeV energy widths centered at $\frac{1}{3}E_{c.m.}$ and $\frac{2}{3}E_{c.m.}$ for the d and α spectra, respectively, are observed [11,29–32]. Gaussian distributions centered at $\frac{1}{3}E_{c.m.}$ and $\frac{2}{3}E_{c.m.}$ were considered for the d and α captured composite systems, respectively. Typical 10 MeV energy widths in α and d spectra were assumed for both the calculations. Two separate calculations assuming these distributions were performed. The calculated values of absolute cross sections for the residues from d capture ^{124,125}Sb are plotted in Fig. 6, showing reasonably good agreement with the data. Similarly the calculations for ^{126,127}Te residues from α capture are shown in Fig. 6(b), showing a similar agreement. These calculations suggest that these residues are populated via fragment capture or transfer followed by evaporation, not through any other one-step direct process.

TABLE III. Cross sections for α capture in the ^{6}Li + ^{159}Tb system. The 1n (^{162}Ho) and 3n (^{160}Ho) channel cross sections are measured in the present study, while the 2n (^{161}Ho) channel cross sections are taken from Ref. [18].

E_{lab} (MeV)	^{162}Ho (present work) (mb)	^{161}Ho [18] (mb)	^{160}Ho (present work) (mb)	^{Tot}Ho (mb)
23.7	5.07 ± 0.72			5.07 ± 0.72
25.8	15.6 ± 2.7	7.0 ± 1.1		22.6 ± 2.8
29.8	37.1 ± 5.7	31.7 ± 3.1		68.8 ± 6.2
33.8	23.1 ± 3.8	68.7 ± 5.9	2.14 ± 0.37	94.0 ± 6.0

C. Comparison of ICF cross sections with ^{6,7}Li projectiles

In Figs. 7(a)–7(d), we have plotted the available measured d capture and α capture cross section data as a function of $E_{c.m.}/V_B$ for ^{6}Li projectile on ^{209}Bi [15], ^{197}Au [16], ^{159}Tb [18], and ^{124}Sn (present data) targets, respectively. Here, the values of V_B used were calculated in CCFULL code, which adds the Coulomb and nuclear potentials, the later is given in the form of Akyuz Winther potentials [23]. It is observed that with ^{209}Bi and ^{197}Au targets, d capture dominates over α capture at below barrier while α capture and d capture are of similar order at above-barrier energies. However, with ^{159}Tb [18], and ^{124}Sn data, it is seen that the d capture is dominant over α capture at all energies. It is observed that in the ^{209}Bi and ^{197}Au measurements, some of the residues from d capture were not measured, hence d capture is lower than α capture cross sections at above-barrier energies.

Similarly, in Figs. 7(e)–7(h), we have plotted the available measured t capture and α capture data with ^{7}Li projectile on ^{209}Bi [15], ^{197}Au [16], ^{159}Tb [17], and ^{124}Sn [14] targets, respectively. Here it is observed that the cross sections for t capture are dominant over α capture at all the energies. Similar observations were also reported in our earlier works [10,12,13]. There can be two reasons for the dominance of d/t capture over α capture : (i) Q values for d/t capture are much more than α capture for all the reactions considered and (ii) The Coulomb barrier for d capture is lower than that of α capture on same target. These two cumulative effects favor d/t capture over α capture.

Comparison of the d and t capture cross sections with ^{6,7}Li projectiles on the same target reveals that d capture cross sections are larger than t capture cross sections at below-barrier energies, while at energies above the barrier they are similar, except for ^{209}Bi and ^{197}Au targets (due to missing residue cross sections from d capture).

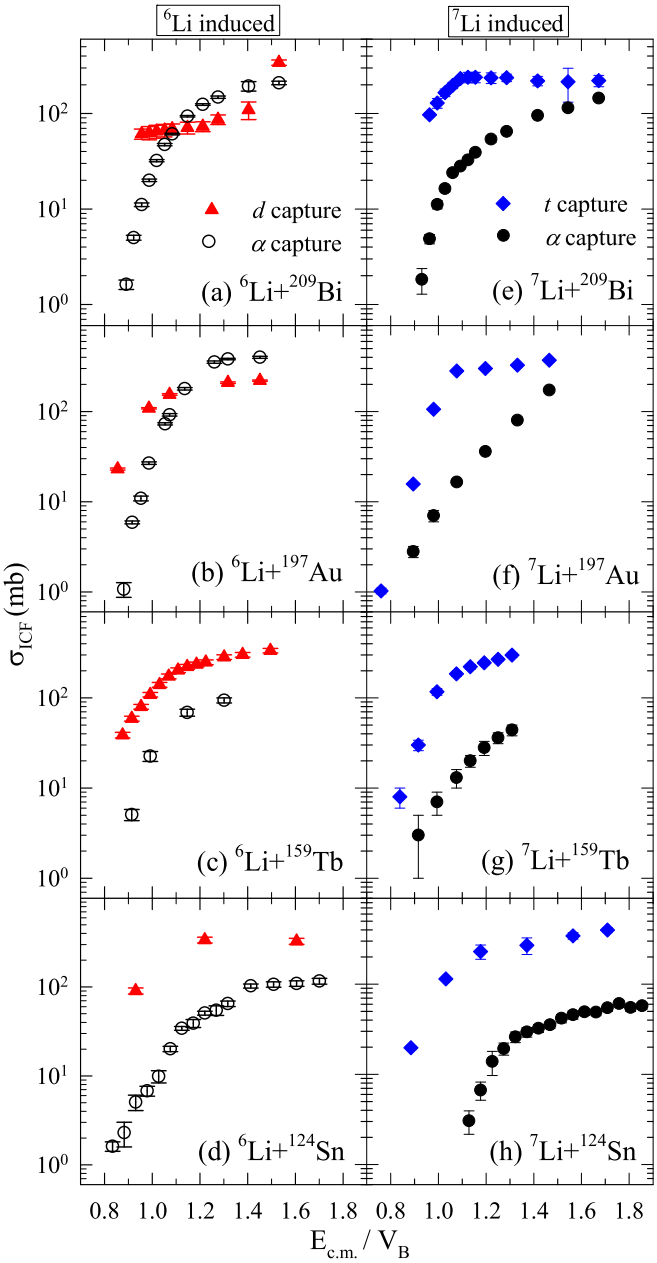

FIG. 7. (a)–(d) Measured d capture and α capture cross sections as a function of $E_{c.m.}/V_B$ for (a)^{6}Li + ^{209}Bi [15], (b)^{6}Li + ^{197}Au [16], (c) ^{6}Li + ^{159}Tb [18], and (d) ^{6}Li + ^{124}Sn (present data) systems are shown with filled triangle and hollow circle symbols respectively. (e)–(h) Measured t capture and α capture cross sections as a function of $E_{c.m.}/V_B$ for (a)^{7}Li + ^{209}Bi [15], (b)^{7}Li + ^{197}Au [16], (c) ^{7}Li + ^{159}Tb [17], and (d) ^{7}Li + ^{124}Sn [14] systems are shown with filled diamond and filled circle symbols respectively.

D. Systematics of total fusion with ^{6,7}Li projectiles

For fusion of weakly bound nuclei on light and medium mass targets, the same residue can be populated by the CF and ICF mechanisms, making their separation much more difficult. For this reason, most of the fusion data for light and medium mass systems are relative to total fusion (TF). In the previous works on ^{6,7}Li projectiles with light and medium mass targets,

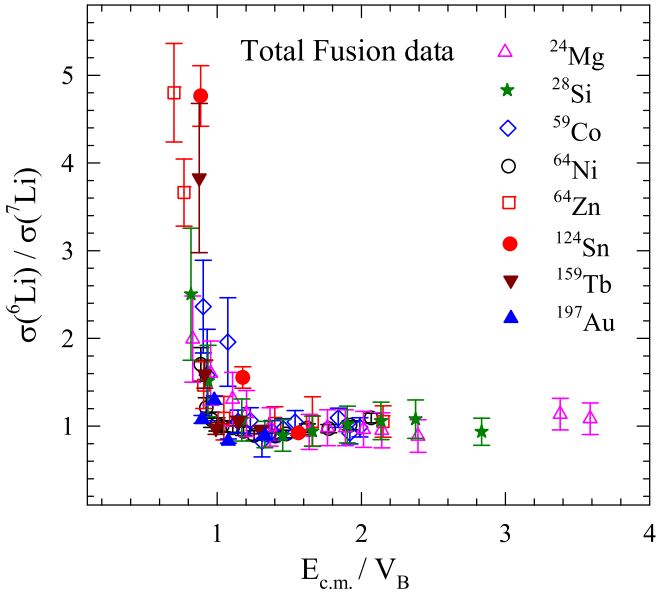

FIG. 8. Ratio of the ^{6}Li to ^{7}Li induced total fusion excitation functions as a function of $E_{c.m.}/V_B$. The present data of ^{124}Sn (solid circles) are compared with other targets taken from Refs. [16–18,35,37,38]. (See text for details.)

viz., ^{24}Mg [33], ^{28}Si [34,35], ^{59}Co [36], ^{64}Zn [37], ^{64}Ni [38], it was observed that the ratio of the measured TF cross sections of ^{6}Li to ^{7}Li as a function of reduced energy $E_{c.m.}/V_B$ gives a universal behavior as shown in Fig. 8. In the above-barrier region the ratio is nearly unity, but as the energy decreases below the barrier it exhibits a rising trend for all the systems. Here the experimental data and values of V_B used were taken from Refs. [35,37,38].

For heavier mass targets, the CF and ICF contributions can be separated out and hence TF can be defined as an addition of CF and ICF cross sections. Because in the present set of data with the ^{124}Sn target the CF and ICF cross sections are available, we have plotted the TF cross section ratio in Fig. 8. We have also extracted the CF and ICF data available with ^{159}Tb [17,18] and ^{197}Au [16] targets and plotted them in Fig. 8. It is interesting to see the similar rising trend at below-barrier energies and near unity at above-barrier energies with all these heavy mass targets also. The rising trend at below-barrier energies can be justified since ICF cross sections (mainly d capture) with the ^{6}Li projectile are larger than those (mainly t capture) with the ^{7}Li projectile, as demonstrated in the previous section.

E. Simultaneous description of CF, ICF, and TF cross sections

Several models employing both classical and quantum mechanical methods have been used to investigate the CF and ICF processes for reactions with weakly bound nuclei [12,39–48]. In a quantum mechanical treatment like the continuum discretized coupled channel (CDCC) approach, coupled channel effects of the projectile breakup are taken care of exactly and utilized to understand CF and ICF processes [12,42–45]. Several experimental studies in recent times have

indicated the importance of indirect paths contributing to breakup and ICF [49]. In recent classical trajectory model calculations [39–41], an attempt has been made to understand the sequential fusion from other processes after breakup. An explicit treatment of all these sequential processes which lead to a large number of final states through various mechanisms in a full quantum mechanical framework is a daunting task. In this regard, an inclusive breakup model has been developed by Lei and Moro [48], which incorporates the sum over all the possible final states through which the unobserved fragment may interact with the target. A good description of the inclusive α breakup cross sections for ^{6}Li induced reactions has been obtained in this calculation. The indirect processes, which may include processes such as the breakup fusion or the exchange of nucleons between the fragment and the target, can also be studied through the effects of imaginary potentials describing the absorption of these fragments in the CDCC calculation. This method was employed in our earlier works [12–14] to obtain a simultaneous description of complete, incomplete, and total fusion cross sections around Coulomb barrier energies for the ^{6,7}Li projectiles on several targets. Recently, similar calculations for CF and ICF cross sections were also reported by Camacho *et al.* [50] for the ^{6}Li + ^{144}Sm,^{154}Sm systems. Coupled channels calculations using CDCC method with the code FRESCO (version 2.9) [51] are performed here for the present set of data for the ^{6}Li + ^{124}Sn system. The details of the calculation method were already described in the earlier work [12] and only a short summary pertaining to this work is presented here.

In the calculations, we assume the cluster structure of $^{6}\mathrm{Li} \rightarrow \alpha + d$ ($E_{\mathrm{thres}} = 1.47$ MeV), and the binding potential for $\alpha - d$ in ^{6}Li was taken from Ref. [52]. The real ($V_{\alpha-T}$ and V_{d-T}) potentials as well as the short-range imaginary ($W_{\alpha-T}$ and W_{d-T}) volume type potentials were used for the interactions between fragments and the target. In addition, another short-range imaginary volume type potential W_{P-T} in the ^{6}Li-target channel is introduced. The density dependent double folding São Paulo potentials (SPPs) [53] were used for $V_{\alpha-T}$ and V_{d-T}, while the short-range imaginary potentials for α + target (d + target) were $W_0 = 25$ (25) MeV, $r_w = 0.59$ (0.74) fm, $a_w = 0.4$ (0.4) fm. With these potentials, the total fusion cross section (σ_{TF}) was calculated. In the calculations, we use the parameters as $W_{P-T} = 25$ MeV, $r_{P-T} = 1.0$ fm, and $a_{P-T} = 0.4$ fm. This imaginary potential ensures that the total flux decreases by the absorption when the core and the valence cluster are in the range of the potential of target nucleus. Small regions of absorption of $W_{\alpha-T}$ and W_{d-T} as compared to W_{P-T} reduces the possible double counting effects. Incomplete fusion cross sections for d capture and α capture were determined by turning off the imaginary potentials W_{d-T} and $W_{\alpha-T}$ respectively, as described in earlier works [12,14]. Then total incomplete fusion can be obtained by adding $\sigma_{\alpha\,\mathrm{capture}}$ and $\sigma_{d\,\mathrm{capture}}$, and complete fusion can be determined by $\sigma_{\mathrm{CF}} = \sigma_{\mathrm{TF}} - \sigma_{\mathrm{ICF}}$.

In Fig. 9(a) results of the calculations for the TF, CF, and ICF cross sections are shown with long dashed, short dashed, and dotted lines, respectively, along with the corresponding experimental data. The bare calculations (without breakup couplings) were also performed and the calculated fusion cross

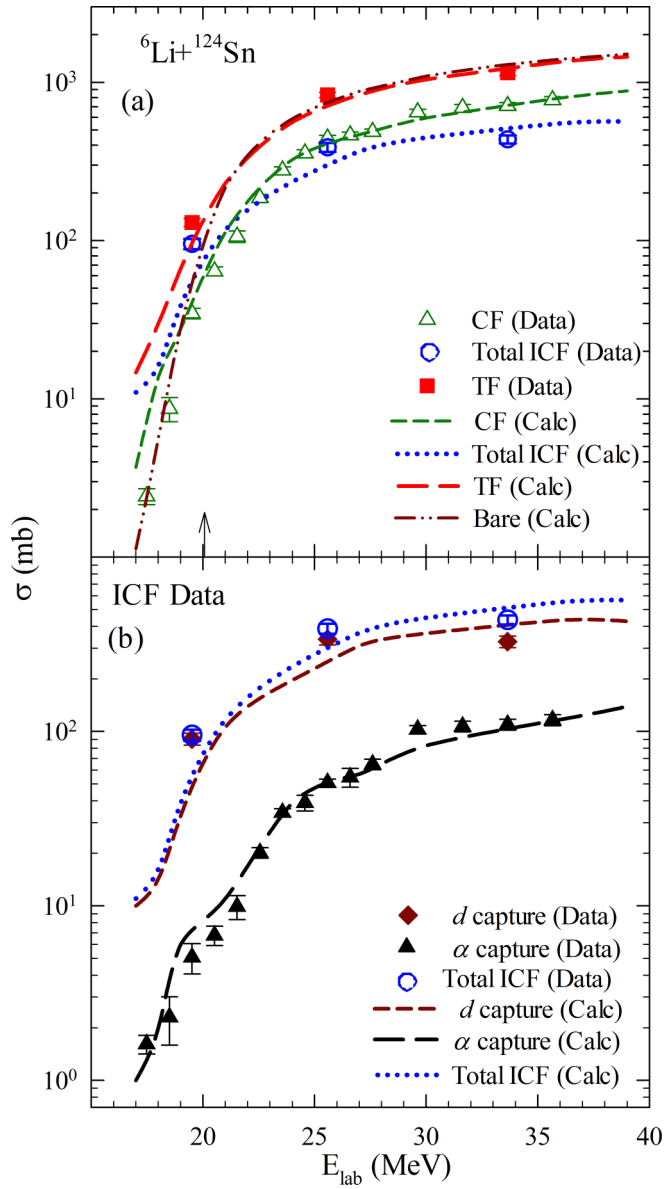

FIG. 9. (a) The data of CF, ICF, and TF cross sections for ^{6}Li + ^{124}Sn system are compared with the coupled channel calculations. The arrow indicate the position of the Coulomb barrier. (b) Comparison of individual ICF contributions from α capture and d capture along with total ICF with the calculations. (See text for details.)

sections are denoted by a dash-dot-dot line. The Coulomb barrier position is marked by an arrow in the figure. It is seen that, at energies above the Coulomb barrier, the calculations which include the couplings and calculations that omit them have negligible difference, but, at energies below the barrier, the coupled TF cross sections are enhanced in comparison to bare TF cross sections. The calculated individual ICF cross sections, $\sigma_{\alpha\,\mathrm{capture}}$ and $\sigma_{d\,\mathrm{capture}}$, are shown in Fig. 9(b) along with the measured data. The simultaneous description of CF, individual ICF, and total ICF was achieved from these coupled channels calculations.

The ratios of cross sections, $\sigma_{\mathrm{ICF}}/\sigma_{\mathrm{TF}}$ and $\sigma_{\mathrm{CF}}/\sigma_{\mathrm{TF}}$, derived from the calculations as a function of $E_{\mathrm{c.m.}}/V_{\mathrm{B}}$ for the

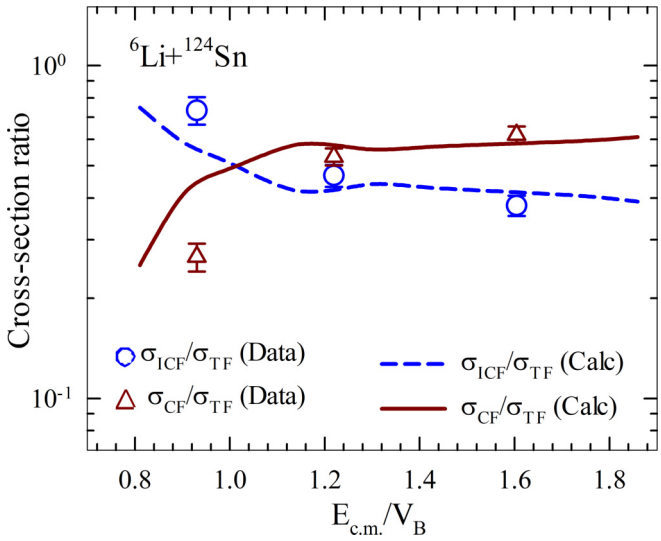

FIG. 10. The ratios of cross sections, σ_{ICF}/σ_{TF} and σ_{CF}/σ_{TF}, derived from the calculations as a function of $E_{c.m.}/V_B$ for the ^{6}Li + ^{124}Sn system are shown by dashed and solid lines respectively. The symbols show the experimental data.

^{6}Li + ^{124}Sn system are shown in Fig. 10. The corresponding experimental data from the present measurement of σ_{ICF}/σ_{TF} and σ_{CF}/σ_{TF} are also shown in Fig. 10. From the figure it is evident that σ_{ICF}/σ_{TF} and σ_{CF}/σ_{TF} ratios remain approximately constant over the energy range above the barrier and CF is dominant over ICF. For energies below the barrier, the σ_{ICF}/σ_{TF} ratio is increasing while the σ_{CF}/σ_{TF} ratio is decreasing. This shows the dominance of ICF at below-barrier energies. At the barrier position, σ_{ICF}/σ_{TF} and σ_{CF}/σ_{TF} ratios are of similar magnitude, indicating the equal importance of CF and ICF. The σ_{ICF}/σ_{TF} ratio at above-barrier energies gives a value of the suppression factor in CF which is found to be in agreement (∼40%) with the literature data for ^{6}Li projectiles from various measurements [3–5], and in agreement with the value for CF suppression factor obtained with the CCFULL calculations. Hence simultaneous measurement of CF and ICF cross sections is essential for understanding of the CF suppression factor.

IV. SUMMARY

Complete and incomplete fusion along with one neutron transfer excitation functions for the ^{6}Li + ^{124}Sn system were measured in the energy range $0.9 < E_{c.m.}/V_B < 1.7$ by online and offline γ-ray detection techniques. At above-barrier energies, the measured complete fusion cross sections were found to be suppressed by a factor of $34 \pm 4\%$ in comparison with the coupled channel calculations performed using the model adopted in CCFULL. This suppression factor is found to be in agreement with the literature data for the ^{6}Li projectile on various targets. The CF cross sections for the present system were compared with the previously measured ^{7}Li + ^{124}Sn [14] system. It was found that at below-barrier (above-barrier) energies, CF cross sections with ^{6}Li are larger (smaller) than with the ^{7}Li projectile.

The measured d capture cross sections in ^{6}Li + ^{124}Sn and ^{6}Li + ^{159}Tb systems were found to be significantly more than the α capture cross sections at all the energies, contrary to the observations for the ^{6}Li + ^{209}Bi [15] and ^{6}Li + ^{197}Au [16] systems. The statistical model calculations successfully explain the measured cross sections for the residues arising from d capture and α capture in the ^{6}Li + ^{124}Sn system. These calculations suggest that these residues are populated via fragment capture or transfer followed by evaporation, not through any other one-step direct process. The measured ICF cross sections taken as sum of d capture and α capture cross sections are found to be commensurate with the suppression observed in the CF data. Further, simultaneous measurements of CF and ICF preferably with different target mass systems are required to understand these aspects.

The TF cross section ratios of ^{6}Li to ^{7}Li induced reactions on several targets showed a universal behavior. In the above-barrier region, the ratio is nearly unity, but as the energy decreases below the barrier it exhibits a rising trend. The data reveal that the ICF cross sections (mainly d capture) with the ^{6}Li projectile are larger than those (mainly t capture) with the ^{7}Li projectile at below-barrier energies and hence this causes the rising trend at below-barrier energies.

We also performed the CDCC based coupled channel calculations, which include the coupling of breakup continuum of the ^{6}Li nucleus explicitly using cluster folding potentials in the real part along with short-range imaginary potentials to calculate the CF, ICF, and TF cross sections. A simultaneous explanation of the experimental data for the CF, ICF, and TF cross sections over the entire energy range was obtained. It will be interesting to study the relative importance of the breakup and transfer contributing to the ICF and extract the distinguishing characteristics of these two processes. The calculated and experimental ICF fraction, which is the ratio of ICF and TF cross sections, is found to be constant at energies above the barrier and it increases at energies below the barrier, showing the enhanced importance of the ICF contribution in TF at below-barrier energies.

ACKNOWLEDGMENTS

The authors would like to thank the Pelletron-Linac accelerator staff for providing a steady and uninterrupted beam and Mr. P. Patale for help during the experiment. We also thank Prof. J. Lubian for giving us the code to calculate São Paulo potentials. One of the authors (V.V.P.) acknowledges financial support through a Young Scientist Research grant, from the Indian National Science Academy, Government of India, in carrying out these investigations.

[1] L. F. Canto, P. R. S. Gomes, R. Donangelo, J. Lubian, and M. S. Hussein, Phys. Rep. **596**, 1 (2015).

[2] N. Keeley, N. Alamanos, K. W. Kemper, and K. Rusek, Prog. Part. Nucl. Phys. **63**, 396 (2009).

[3] V. V. Parkar, R. Palit, S. K. Sharma, B. S. Naidu, S. Santra, P. K. Joshi, P. K. Rath, K. Mahata, K. Ramachandran, T. Trivedi, and A. Raghav, Phys. Rev. C **82**, 054601 (2010).

[4] B. Wang, W.-J. Zhao, P. R. S. Gomes, E.-G. Zhao, and S.-G. Zhou, Phys. Rev. C **90**, 034612 (2014).

[5] A. Kundu, S. Santra, A. Pal, D. Chattopadhyay, B. K. Nayak, A. Saxena, and S. Kailas, Phys. Rev. C **94**, 014603 (2016).

[6] H. Kumawat, V. Jha, B. J. Roy, V. V. Parkar, S. Santra, V. Kumar, D. Dutta, P. Shukla, L. M. Pant, A. K. Mohanty, R. K. Choudhury, and S. Kailas, Phys. Rev. C **78**, 044617 (2008).

[7] P. R. S. Gomes, M. D. Rodríguez, G. V. Martí, I. Padron, L. C. Chamon, J. O. Fernández Niello, O. A. Capurro, A. J. Pacheco, J. E. Testoni, A. Arazi, M. Ramírez, R. M. Anjos, J. Lubian, R. Veiga, R. Liguori Neto, E. Crema, N. Added, C. Tenreiro, and M. S. Hussein, Phys. Rev. C **71**, 034608 (2005).

[8] S. Santra, S. Kailas, K. Ramachandran, V. V. Parkar, V. Jha, B. J. Roy, and P. Shukla, Phys. Rev. C **83**, 034616 (2011).

[9] H. Kumawat, V. Jha, V. V. Parkar, B. J. Roy, S. Santra, V. Kumar, D. Dutta, P. Shukla, L. M. Pant, A.K. Mohanty, R. K. Choudhury, and S. Kailas, Phys. Rev. C **81**, 054601 (2010).

[10] S. K. Pandit, A. Shrivastava, K. Mahata, V. V. Parkar, R. Palit, N. Keeley, P. C. Rout, A. Kumar, K. Ramachandran, S. Bhattacharyya, V. Nanal, C. S. Palshetkar, T. N. Nag, S. Gupta, S. Biswas, S. Saha, J. Sethi, P. Singh, A. Chatterjee, and S. Kailas, Phys. Rev. C **96**, 044616 (2017).

[11] S. Santra, S. Kailas, V. V. Parkar, K. Ramachandran, V. Jha, A. Chatterjee, P. K. Rath, and A. Parihari, Phys. Rev. C **85**, 014612 (2012).

[12] V. V. Parkar, V. Jha, and S. Kailas, Phys. Rev. C **94**, 024609 (2016).

[13] V. V. Parkar, V. Jha, and S. Kailas, EPJ Web Conf. **163**, 00044 (2017).

[14] V. V. Parkar, S. K. Sharma, R. Palit, S. Upadhyaya, A. Shrivastava, S. K. Pandit, K. Mahata, V. Jha, S. Santra, K. Ramachandran, T. N. Nag, P. K. Rath, B. Kanagalekar, and T. Trivedi, Phys. Rev. C **97**, 014607 (2018).

[15] M. Dasgupta, P. R. S. Gomes, D. J. Hinde, S. B. Moraes, R. M. Anjos, A. C. Berriman, R. D. Butt, N. Carlin, J. Lubian, C. R. Morton, J. O. Newton, and A. Szanto de Toledo, Phys. Rev. C **70**, 024606 (2004).

[16] C. S. Palshetkar, S. Thakur, V. Nanal, A. Shrivastava, N. Dokania, V. Singh, V. V. Parkar, P. C. Rout, R. Palit, R. G. Pillay, S. Bhattacharyya, A. Chatterjee, S. Santra, K. Ramachandran, and N. L. Singh, Phys. Rev. C **89**, 024607 (2014).

[17] R. Broda, M. Ishihara, B. Herskind, H. Oeschler, S. Ogaza, and H. Ryde, Nucl. Phys. A **248**, 356 (1975).

[18] M. K. Pradhan, A. Mukherjee, P. Basu, A. Goswami, R. Kshetri, S. Roy, P. Roy Chowdhury, M. Saha Sarkar, R. Palit, V. V. Parkar, S. Santra, and M. Ray, Phys. Rev. C **83**, 064606 (2011).

[19] B. Ding, Y. H. Zhang, X. H. Zhou, G. X. Dong, F. R. Xu, M. L. Liu, G. S. Li, N. T. Zhang, H. X. Wang, H. B. Zhou, Y. J. Ma, Y. Sasakiz, K. Yamada, H. Ohshima, S. Yokose, M. Ishizuka, T. Komatsubara, and K. Furuno, Phys. Rev. C **85**, 044306 (2012).

[20] B. Kanagalekar, P. Das, B. Bhujang, S. Muralithar, R. P. Singh, and R. K. Bhowmik, Phys. Rev. C **88**, 054306 (2013).

[21] A. Gavron, Phys. Rev. C **21**, 230 (1980).

[22] K. Hagino, N. Rowley, and A. T. Kruppa, Comput. Phys. Commun. **123**, 143 (1999).

[23] R. A. Broglia and A. Winther, in *Heavy Ion Reactions*, Lecture Notes Vol. I (Addison-Wesley, Redwood City, CA, 1991), p. 114.

[24] T. Kibedi and R. H. Spear, At. Data Nucl. Data Tables **80**, 35 (2002).

[25] P. K. Rath, S. Santra, N. L. Singh, R. Tripathi, V. V. Parkar, B. K. Nayak, K. Mahata, R. Palit, S. Kumar, S. Mukherjee, S. Appannababu, and R. K. Choudhury, Phys. Rev. C **79**, 051601(R) (2009).

[26] P. K. Rath, S. Santra, N. L. Singh, B. K. Nayak, K. Mahata, R. Palit, K. Ramachandran, S. K. Pandit, A. Parihari, A. Pal, S. Appannababu, S. K. Sharma, D. Patel, and S. Kailas, Phys. Rev. C **88**, 044617 (2013).

[27] C. T. Zhang, P. Bhattacharyya, P. J. Daly, Z. W. Grabowski, R. H. Mayer, M. Sferrazza, R. Broda, B. Fornal, W. Krolas, T. Pawlat, D. Bazzacco, S. Lunardi, C. Rossi Alvarez, and G. de Angelis, Nucl. Phys. A **628**, 386 (1998).

[28] S. K. Pandit, Ph.D. thesis (2018), HBNI, Mumbai (unpublished).

[29] A. Shrivastava, A. Navin, A. Diaz-Torres, V. Nanal, K. Ramachandran, M. Rejmund, S. Bhattacharyya, A. Chatterjee, S. Kailas, A. Lemasson, R. Palit, V. V. Parkar, R. G. Pillay, P. C. Rout, and Y. Sawant, Phys. Lett. B **718**, 931 (2013).

[30] K. O. Pfeiffer, E. Speth, and K. Bethge, Nucl. Phys. A **206**, 545 (1973).

[31] C. Signorini, A. Edifizi, M. Mazzocco, M. Lunardon, D. Fabris, A. Vitturi, P. Scopel, F. Soramel, L. Stroe, G. Prete, E. Fioretto, M. Cinausero, M. Trotta, A. Brondi, R. Moro, G. LaRana, E. Vardaci, A. Ordine, G. Inglima, M. LaCommara, D. Pierroutsakou, M. Romoli, M. Sandoli, A. Diaz-Torres, I. J. Thompson, and Z. H. Liu, Phys. Rev. C **67**, 044607 (2003).

[32] M. K. Pradhan, A. Mukherjee, S. Roy, P. Basu, A. Goswami, R. Kshetri, R. Palit, V. V. Parkar, M. Ray, M. SahaSarkar, and S. Santra, Phys. Rev. C **88**, 064603 (2013).

[33] M. Ray, A. Mukherjee, M. K. Pradhan, R. Kshetri, M. S. Sarkar, R. Palit, I. Majumdar, P. K. Joshi, H. C. Jain, and B. Dasmahapatra, Phys. Rev. C **78**, 064617 (2008).

[34] A. Pakou, K. Rusek, N. Alamanos, X. Aslanoglou, M. Kokkoris, A. Lagoyannis, T. J. Mertzimekis, A. Musumarra, N. G. Nicolis, D. Pierroutsakou, and D. Roubos, Eur. Phys. J A **39**, 187 (2009).

[35] M. Sinha, H. Majumdar, P. Basu, S. Roy, R. Bhattacharya, M. Biswas, M. K. Pradhan, R. Palit, I. Mazumdar, and S. Kailas, Eur. Phys. J A **44**, 403 (2010).

[36] C. Beck, F. A. Souza, N. Rowley, S. J. Sanders, N. Aissaoui, E. E. Alonso, P. Bednarczyk, N. Carlin, S. Courtin, A. Diaz-Torres, A. Dummer, F. Haas, A. Hachem, K. Hagino, F. Hoellinger, R. V. F. Janssens, N. Kintz, R. Liguori Neto, E. Martin, M. M. Moura, M. G. Munhoz, P. Papka, M. Rousseau, A. Sanchezi Zafra, O. Stezowski, A. A. Suaide, E. M. Szanto, A. Szanto de Toledo, S. Szilner, and J. Takahashi, Phys. Rev. C **67**, 054602 (2003).

[37] A. Di Pietro, P. Figuera, E. Strano, M. Fisichella, O. Goryunov, M. Lattuada, C. Maiolino, C. Marchetta, M. Milin, A. Musumarra, V. Ostashko, M. G. Pellegriti, V. Privitera, G. Randisi, L. Romano, D. Santonocito, V. Scuderi, D. Torresi, and M. Zadro, Phys. Rev. C **87**, 064614 (2013).

[38] Md. M. Shaikh, S. Roy, S. Rajbanshi, A. Mukherjee, M. K. Pradhan, P. Basu, V. Nanal, S. Pal, A. Shrivastava, S. Saha, and R. G. Pillay, Phys. Rev. C **93**, 044616 (2016).

[39] M. Boseli and A. Diaz-Torres, J. Phys. G **41**, 094001 (2014).

[40] A. Diaz-Torres, Comput. Phys. Commun. **182**, 1100 (2011).

[41] A. Diaz-Torres and D. Quraishi, Phys. Rev. C **97**, 024611 (2018).

[42] A. Diaz-Torres and I. J. Thompson, Phys. Rev. C **65**, 024606 (2002).

[43] A. Diaz-Torres, I. J. Thompson, and C. Beck, Phys. Rev. C **68**, 044607 (2003).

[44] V. Jha, V. V. Parkar, and S. Kailas, Phys. Rev. C **89**, 034605 (2014).
[45] S. Hashimoto, K. Ogata, S. Chiba, and M. Yahiro, Prog. Theor. Phys. **122**, 1291 (2009).
[46] J. Lei and A. M. Moro, Phys. Rev. C **92**, 044616 (2015).
[47] A. M. Moro and J. Lei, Few-Body Syst. **57**, 319 (2016).
[48] J. Lei and A. M. Moro, Phys. Rev. C **95**, 044605 (2017).
[49] K. J. Cook, I. P. Carter, E. C. Simpson, M. Dasgupta, D. J. Hinde, L. T. Bezzina, S. Kalkal, C. Sengupta, C. Simenel, B. M. A. Swinton-Bland, K. Vo-Phuoc, and E. Williams, Phys. Rev. C **97**, 021601(R) (2018).
[50] A. Gómez Camacho, J. Lubian, H. Q. Zhang, and S.-G. Zhou, Chin. Phys. C **41**, 124103 (2017).
[51] I. J. Thompson, Comput. Phys. Rep. **7**, 167 (1988).
[52] K. I. Kubo and M. Hirata, Nucl. Phys. A **187**, 186 (1972).
[53] L. C. Chamon, B. V. Carlson, L. R. Gasques, D. Pereira, C. De Conti, M. A. G. Alvarez, M. S. Hussein, M. A. Candido Ribeiro, E. S. Rossi, and C. P. Silva, Phys. Rev. C **66**, 014610 (2002).